Optical and Quantum Electronics **15** *(1983) 325–347*

Theoretical analysis of S_1-state lifetime measurements of dyes with picosecond laser pulses

A. PENZKOFER, W. BLAU
Naturwissenschaftliche Fakultät II – Physik, Universität Regensburg, 8400 Regensburg, Federal Republic of Germany

Received 22 November 1982

Various methods for the determination of the S_1-state lifetime of dye solutions (laser dyes and mode-locking dyes) are analysed. A general model of interaction of laser light with dye molecules is presented and reduced to a dye energy level scheme of six levels. Fluorescence emission, light amplification and absorption recovery techniques are investigated theoretically and their limitations revealed. The determination of the S_1-state lifetime of saturable absorbers by single picosecond pulse bleaching experiments is very thoroughly discussed. The influence of various laser and dye parameters on the bleaching experiments are analysed numerically. The results are compared with isotropic steady state two- and three-level dye models.

1. Introduction

The S_1-singlet state lifetime is one of the key parameters of dyes used as active laser media or as saturable absorbers [1]. Laser dyes require S_1-state lifetimes close to the radiative lifetime, i.e. a fluorescence quantum yield near to one (negligble radiationless relaxation). Saturable absorbers when used as mode-locking dyes should exhibit fast radiationless decay channels from S_1 to S_0 [2].

Various techniques have been used to measure the S_1-state lifetime of dyes. The methods apply either spontaneous emission (fluorescence), stimulated emission (amplification of probe pulse) or absorption changes.

The fluorescence lifetime measurements can be subdivided according to excitation source and detection technique [3, 4].

1. Phase fluorimetry requires a modulated excitation source (cw light source and external modulation [5, 6], two-mode operation of cw gas laser [7, 8], cw mode-locked laser [9, 10]) and phase sensitive detection (lock-in). It allows the measurement of fluorescence lifetimes down to the picosecond region. The functional form of the decay curve has to be assumed (e.g. single exponential decay).

2. Time correlated single photon counting techniques (delayed coincidence techniques) apply repetitive flash excitation (ps light pulses [11, 12], ns pulses with a cut-off trailing edge [13]) and photomultiplier detectors together with pulse height discriminators and start-stop multichannel analysers. The time resolution reaches as far as the subnanosecond region.

3. Dye excitation with intense picosecond pump pulses allows single shot fluorescence decay measurements with fast photodetectors and travelling-wave oscilloscopes [14–16]. The time resolution is restricted to the nanosecond region. In the case of dye excitation with cw mode-locked lasers, fast photodetectors and sampling oscilloscopes [17] or boxcar integrating techniques [18] bring the time resolution down to the subnanosecond range.

4. Fluorescence lifetimes in the picosecond time region are frequently measured with streak cameras [2]. In single shot experiments, an intense picosecond pump pulse excites the molecules and the fluor-

0306-8919/83 $03.00 + .12.

escence signal is registered with a triggered streak tube [19, 20]. For cw mode-locked laser excitation a synchronously operated streak camera facilitates recording and increases dynamic range [21].

5. Instead of the streak camera, various gating techniques are available for picosecond time resolved fluorescence detection. These methods include the optical Kerr gate [22, 23], the saturable absorber gate [24], and the sum or difference frequency mixing of a delayed probe pulse with fluorescence emission [25–29].

6. Besides time resolved fluorescence decay measurements, the S_1-state lifetime may be inferred from fluorescence quantum yield measurements and calculations of the radiative lifetime [30]. This technique is independent of the excitation pulse duration. Lifetimes down to the subpicosecond range may be deduced.

Stimulated emission has been applied to lifetime measurements in picosecond pump and time-delayed picosecond probe experiments [31]. The probe pulse frequency has to be in the S_1–S_0 fluorescence band in order to be amplified by the S_1-state population. Lifetimes longer than the involved pulse durations are measurable.

Intense excitation pulses bleach the ground state absorption [2]. The absorption recovery which is related to the S_1-state lifetime may be measured by a time delayed probe pulse [16, 32–35]. Lifetimes longer than the pump pulse duration are accessible. For lifetimes comparable to or shorter than the pump pulse duration, the excited state lifetime may be inferred from transmission measurements of the pump pulse [36–39]. The faster the molecules return to the ground state the more difficult it will be to bleach the dyes. The depopulation of the S_1-state may also be probed by time-delayed excited state absorption measurements [40].

In this paper we first present a general model for the interaction of light with dye molecules and the relaxation of excited molecules. The resulting complex system of equations is simplified using reasonable assumptions that are good approximations in many cases. The equations derived are applied to various techniques of S_1-state lifetime measurements such as spontaneous emission, stimulated emission and absorption detection. The limits of the methods are revealed. The technique of nonlinear transmission of a single pump pulse is very thoroughly discussed. The influence of various parameters such as pulse duration, temporal and spatial pulse shape, excited state absorption, molecular reorientation, absorption anisotropy, intersystem crossing and amplified spontaneous emission on the energy transmission is analysed. The results obtained are compared with simple isotropic two-level and three-level steady state models [40] which are often employed in the literature [41, 42].

2. Analysis of light interaction with dye molecules

Dye molecules dissolved in solvents are separated into monomers. Only at high dye concentration are dimers and higher aggregates formed [1, 43] (preferably in aqueous solutions). In the S_0-ground state, hindered rotational states and low lying vibrational states are thermally populated. The energy level separation between ground state S_0 and excited singlet state S_1 and triplet state T_1 is in the visible frequency region. The exact ground state to excited state frequency spacing varies for the molecules in solution due to changing liquid arrangement around the dissolved molecules (inhomogeneous broadening). Laser light at a fixed frequency interacts with molecules whose transition frequencies coincide with the laser frequency within the homogeneous linewidth of the particular transition. For a single dye molecule at a well defined ground state level the interaction with laser light may lead to different vibronic excited states in the singlet or triplet system which lie within the homogeneous linewidth. The interaction of light with the complete set of dissolved molecules varies for different molecule groups due to inhomogeneous broadening.

Fig. 1 shows a level scheme for dissolved monomers. The distribution of the energy levels is indicated by the inhomogeneous distribution, g_I, for the bottom level of the triplet state. The distribution g_T represents the thermal population distribution of the S_0-band. The homogeneous distribution function g_H indicates the range of interaction of laser light with nearby levels. A similar level scheme may be drawn for dimers and higher aggregates.

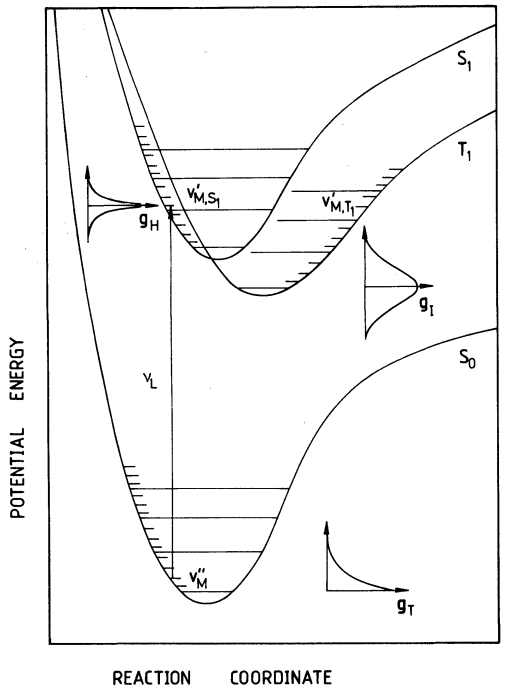

Figure 1 Potential energy diagram of monomeric dye molecules. The curves S_0, S_1 and T_1 represent the potential curves for the singlet ground state S_0, the first excited singlet state S_1 and the lowest triplet state T_1, respectively. The hindered rotational and vibrational states superimposed on the electronic states are indicated. The inset g_T describes the thermal population of eigenstates in the ground state. g_I indicated the inhomogeneous distribution of triplet levels. g_H is the homogeneous line shape and shows the region of levels that are involved in the absorption of light of fixed frequency and fixed ground state level ν''_M. A similar level diagram with shifted levels may be drawn for dimers and higher aggregates.

The interaction of light with dye molecules manifests itself in the absorption spectrum $\alpha(\nu)$. A schematic absorption spectrum for the long-wavelength region which comprises S_0–S_1 singlet–singlet and S_0–T_1 singlet–triplet transitions is shown in Fig. 2. The absorption coefficient, α, at a fixed dye concentration is plotted versus frequency, ν. The absorption spectrum may be sub-divided into a singlet–singlet monomer $\alpha_M(\nu)$, a singlet–singlet dimer $\alpha_D(\nu)$ and a singlet–triplet absorption spectrum

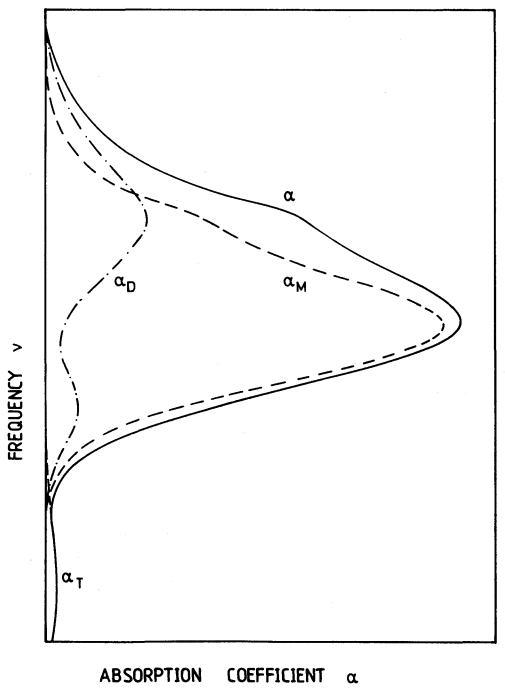

Figure 2 Schematic of lowest frequency absorption band of dye solution. The envelope curve α is composed of S_0–T_1 triplet (α_T), S_0–S_1 monomeric (α_M) and dimeric (α_D) contributions.

$\alpha_T(\nu)$. The triplet absorption maximum is weak and shifted to the long-wavelength side. It is identified as a deviation from the exponential decay of the singlet–singlet absorption on the long-wavelength side of the inhomogeneous line. The separation of the monomer and dimer absorption spectra is accomplished by measuring the absorption spectrum at various dye concentrations [44–46].

At low dye concentrations, $c \lesssim 10^{-5}\,\mathrm{mol\,l^{-1}}$, no dimers are present and the S_0–S_1 absorption, $\alpha(\mathrm{cm^{-1}})$, is determined by the monomer absorption cross-section, $\sigma_M(\mathrm{cm^2})$, i.e. $\alpha(\nu) = cN_A\sigma_M(\nu)/1000$ ($N_A = 6.02205 \times 10^{23}\,\mathrm{mol^{-1}}$, the Avogadro constant). At higher concentration the absorption coefficient is composed of monomer and dimer contributions

$$\alpha = \alpha_M + \alpha_D = \frac{N_A}{1000}(c_M\sigma_M + c_D\sigma_D). \tag{1}$$

The total dye concentration is $c = c_M + 2c_D$. Over a wide concentration range the dimer concentration grows proportional to the square of the total dye concentration, i.e. $c_D = \kappa c^2$, and Equation 1 may be rewritten as

$$\alpha = \frac{N_A c}{1000}[(1 - 2\kappa c)\sigma_M + \kappa c\sigma_D]. \tag{2}$$

The monomer absorption cross-section, $\sigma_M(\nu)$, is determined at low dye concentration. The dimer concentration constant κ is obtained by measuring α at a fixed frequency $\bar{\nu}$ (preferably at the S_0–S_1 absorption maximum) for two dye concentrations c_1, c_2 and solving Equation 2 for κ and $\sigma_D(\bar{\nu})$. After obtaining $\sigma_M(\nu)$ and κ the spectral distribution of $\sigma_D(\nu)$ is calculated from Equation 2.

In special cases distinct monomeric forms may be present in a dye solution, (e.g. acid–base equilibria [47], photoisomers [48]) and these can be resolved in a way similar to the monomer–dimer equilibria [1].

The absorption of linear polarized laser light of frequency ν_L (spectral width $\Delta\nu_L \ll \Delta\nu_H$, $\Delta\nu_L \ll \Delta\nu_I$; $\Delta\nu_H$ is the homogeneous linewidth and $\Delta\nu_I$ the inhomogeneous linewidth) which falls into the long-wavelength absorption band of the dye (S_1, T_1) is generally given by

$$\frac{\partial I_L}{\partial z} + \frac{\eta}{c_0}\frac{\partial I_L}{\partial t} = -I_L\left\{\int_0^{\pi/2} 3\cos^2(\theta) \sum_s \sum_{x,y} \sum_{v_x''} \sum_{v_{x,y}'} \sigma_{s,v_x'',v_{x,y}'}(\nu_L)[N_{s,v_x''}(\theta) - N_{s,v_{x,y}'}(\theta)] \sin\theta\, d\theta \right.$$
$$\left. + \sum_{x,y,w} \sigma_{ex,x,y,w}(\nu_L)N_{x,y}'\right\} \tag{3}$$

where I_L is the pump pulse intensity, η is the refractive index and c_0 the vacuum light velocity. The integration over the angle θ takes care of the absorption anisotropy of electric dipole interaction [49, 50], i.e. the absorption cross-section is given by $\sigma(\theta) = 3\sigma\cos^2(\theta)$. θ is the angle between the direction of the electrical field strength and the direction of the transition dipole moment. σ is the isotropic absorption cross-section. The summations run over the molecular sites s of the inhomogeneous distribution, the aggregates x (x = M for monomers, x = D for dimers), the excited spin states y ($y = S_1$ and $y = T_1$), the rotational-vibrational levels in the ground state (v_x'') and the excited states ($v_{x,y}'$). $N_{s,v_M''}(\theta)$ is the number density of monomer molecules ($\mathrm{cm^{-3}}$) in the rotational-vibrational state v_M'' of the S_0-band and site s with orientation of the transition dipole moment in the θ direction. $N_{s,v_D''}(\theta)$ represents the same quantity for dimer molecules. $N_{s,v_{x,y}'}(\theta)$ is the number density of molecules promoted to the vibronic state $v_{x,y}'$ (x = M or D, $y = S_1$ or T_1) of site s. Prior to laser interaction the excited electronic states are empty [$(N_{s,v_{x,y}'}(\theta) = 0)$] while the ground state levels are isotropic thermally populated, i.e. $N_{s,v_x''}(\theta) = N_{s,v_x''} = N_{s,x}g_T(v_x'')$ with $N_{s,v_x} = \int_0^{\pi/2} N_{s,v_x''}(\theta)\sin\theta\, d\theta$ and $N_{s,x} = \Sigma_{v_x''} N_{s,v_x''} = N_x g_I(s)$. $g_I(s)$ is the inhomogeneous distribution of molecular sites. $N = N_M + N_D$ is the total number density of dye molecules (before laser excitation it is $N_M = N_M''$, $N_D = N_D''$; after excitation it is $N_M = N_M'' + N_{M,S_1}' + N_{M,T_1}' + N_{ex,M,S_n} + N_{ex,M,T_n}$, $N_D = N_D'' + N_{D,S_1}' + N_{D,T_1}' + N_{ex,D,S_n} + N_{ex,D,T_n}$). The absorption of

laser light from the excited states S_1 and T_1 to higher lying levels S_n and T_n is included in Equation 1 by effective excited state absorption cross-sections $\sigma_{ex,x,y,w}$ ($w = S_n$ or T_n). $N'_{x,y} = \int_0^{\pi/2} \Sigma_s \Sigma_{v'_{x,y}} N_{s,v'_{x,y}}(\theta) \sin\theta \, d\theta$ is the number density of molecules excited to the S_1 or T_1 state. A more detailed description of the anisotropy of excited state absorption [51, 52] is not included here.

The population changes of the levels by interaction with laser light are described by the following rate equations.

$$\frac{\partial}{\partial t} N_{s,v''_x}(\theta) = -\frac{3}{h\nu_L} I_L \cos^2(\theta) \sum_y \sum_{v'_{x,y}} \sigma_{s,v''_x,v'_{x,y}}(\nu_L)[N_{s,v''_x}(\theta) - N_{s,v'_{x,y}}(\theta)]$$

$$+ g_T(v''_x) g_I(s) \sum_y \frac{1}{\tau_{F,x,y}} N'_{x,y} - \frac{1}{\tau''_{0,x}} [N_{s,v''_x}(\theta) - N_{s,v''_x}] - \frac{1}{\tau_{s,v''_x}} [N_{s,v''_x}(\theta) - g_T(v''_x) N''_{s,x}(\theta)]$$

$$+ g_T(v''_x) g_I(s) \sum_w k''_{ex,x,w} N_{ex,x,w} \tag{4a}$$

$$\frac{\partial}{\partial t} N''_{s,x}(\theta) = \frac{1}{\tau''_{s,x}} [N''_{s,x}(\theta) - g_I(s) N''_x(\theta)] \tag{4b}$$

$$\frac{\partial}{\partial t} N_{s,v'_{x,y}}(\theta) = \frac{3}{h\nu_L} I_L \cos^2(\theta) \sum_{v''_x} \sigma_{s,v''_x,v'_{x,y}}(\nu_L)[N_{s,v''_x}(\theta) - N_{s,v'_{x,y}}(\theta)] - \frac{1}{\tau_{F,y}} N_{s,v'_{x,y}}(\theta)$$

$$- \frac{1}{\tau'_{0,x}} [N_{s,v'_{x,y}}(\theta) - N_{s,v'_{x,y}}] - \frac{1}{\tau_{s,v'_{x,y}}} [N_{s,v'_{x,y}}(\theta) - g_T(v'_{x,y}) N'_{s,x,y}(\theta)] + g_T(v'_{x,y}) g_I(s)$$

$$\times \sum_w k'_{ex,x,y,w} N_{ex,x,w} - \frac{1}{\tau_{S_1T_1}} N_{s,v'_{x,y}}(\theta) \epsilon_{S_1,y} - \frac{1}{h\nu_L} I_L \sum_w \sigma_{ex,x,y,w} N_{s,v'_{x,y}}(\theta) \tag{5a}$$

$$\frac{\partial}{\partial t} N'_{s,x,y}(\theta) = \frac{1}{\tau'_{s,x,y}} [N'_{s,x,y}(\theta) - g_I(s) N'_{x,y}(\theta)] \tag{5b}$$

$$\frac{\partial}{\partial t} N_{ex,x,w} = \frac{1}{h\nu_L} I_L \sum_y \sigma_{ex,x,y,w}(\nu_L) N'_{x,y} - \sum_y k'_{ex,x,y,w} N_{ex,x,w} - k''_{ex,x,w} N_{ex,x,w}. \tag{6}$$

The absorption and stimulated emission are described by the first terms on the right-hand side of Equations 4a and 5a (h is Planck's constant). The second terms represent the fluorescence (relaxation time τ_{F,x,S_1}) and the phosphorescence (τ_{F,x,T_1}). The third terms take care of molecular reorientation (time constants $\tau''_{0,x}$ in the S_0-ground state, τ'_{0,x,S_1} in the S_1-state, and τ'_{0,x,T_1} in the T_1-state). The fourth terms establish thermal equilibrium of vibronic states at site s in the ground state (time constant τ_{s,v''_x}) and the excited state ($\tau_{s,v'_{x,y}}$). The fifth terms are responsible for relaxation from higher excited states. $k''_{ex,x,w}$ and $k'_{ex,x,y,w}$ are the transition rates of the higher excited states ($w = S_n$ and $w = T_n$) to ground state and first excited electronic states, respectively. The sixth term in Equation 5a takes care of S_1–T_1 intersystem crossing ($\epsilon_{S_1,y} = 1$ for $y = T_1$, $\epsilon_{S_1,y} = 0$ for $y = S_1$). The seventh expression in Equation 5a is responsible for excited state absorption. Equations 4b and 5b describe the molecular site relaxation (spectral cross-relaxation) of disturbed inhomogeneous distribution. $\tau''_{s,x}$ and $\tau'_{s,x,y}$ are the site redistribution time constants. Equation 6 analyses the population of higher lying states S_n ($w = S_n$) and T_n ($w = T_n$) by excited state absorption (first term) and their depopulation by relaxation to S_1 (rate $k'_{ex,x,S_1,w}$) to T_1 ($k'_{ex,x,T_1,w}$) and S_0 ($k''_{ex,x,w}$) ($x = M$ or D, $w = S_n$ or T_n). Amplified spontaneous emission as well as transfer between monomers and dimers is not included in Equations 3–6.

The general Equation system 2–6 includes too many states to be practically tractable. In the following we show, that the states within an electronic band (S_0, S_1, T_1) of a single species (monomer, dimer,

etc.) may be treated as a single level if the vibronic relaxation times τ_{s,v''_x}, $\tau_{s,v'_{x,y}}$ and the cross-relaxation times $\tau''_{s,x}$, $\tau'_{s,x,y}$ are sufficiently fast compared to other temporal changes.

The conditions $\tau_{s,v''_x} = 0$ and $\tau_{s,v'_{x,y}} = 0$ require $N_{s,v''_x}(\theta) = g_T(v''_x)N''_{s,x}(\theta)$ and $N_{s,v'_{x,y}}(\theta) = g_T(v'_{x,y})N'_{x,y}(\theta)$ due to the finite values of the fourth terms of Equations 4a and 5a. The same argument leads to $N''_{s,x}(\theta) = g_I(s)N''_x(\theta)$ and $N'_{s,x,y}(\theta) = g_I(s)N'_{x,y}(\theta)$ for $\tau''_{s,x} = \tau'_{s,x,y} = 0$ (Equations 4b and 5b). Combining both facts gives $N_{s,v''_x}(\theta) = g_T(v''_x)g_I(s)N''_x(\theta)$ and $N_{s,v'_{x,y}}(\theta) = g_T(v'_{x,y})g_I(s)N'_{x,y}(\theta)$. The light absorption promotes molecules from a ground state level to a corresponding Franck–Condon level in the excited state. These Franck–Condon states relax very fast according to the above assumptions of $\tau_{s,v'_{x,y}} \to 0$ and $\tau'_{s,x,y} \to 0$. A refilling of Franck–Condon states in the S_1 and T_1 band by cross-relaxation and thermal population may often be neglected in experiments (small thermally relaxed population of Franck–Condon states). This approximation leads to $N_{s,v'_{x,y}} \to 0$ for the relevant Franck–Condon absorption states.

Equation 3 reduces to

$$\frac{\partial}{\partial z} I_L + \frac{n}{c_0}\frac{\partial I_L}{\partial t} = -I_L\left[\int_0^{\pi/2} 3\cos^2\theta \sum_x \sigma_x(\nu_L)N''_x(\theta)\sin\theta\,d\theta + \sum_{x,y,w} \sigma_{ex,x,y,w}N'_{x,y}\right] \tag{7}$$

with an average absorption cross-section

$$\sigma_x(\nu_L) = \sum_y \sigma_{x,y}(\nu_L) = \sum_s \sum_y \sum_{v''_x} \sum_{v'_{x,y}} \sigma_{s,v''_x,v'_{x,y}}(\nu_L)g_T(v''_x)g_I(s) = \alpha_x(\nu_L)/N_x. \tag{8}$$

The kinetics of the total population of the ground state species $N''_x(\theta) = \Sigma_s\Sigma_{v''_x}N_{s,v''_x}(\theta)$ and of the excited S_1 and T_1-states $N'_{x,y}(\theta) = \Sigma_s\Sigma_{v'_{x,y}}N_{s,v'_{x,y}}(\theta)$ is found by adding Equations 4a and 5a over all rotational-vibrational states and being aware of the fact that vibronic decay and cross-relaxation terms do not appear for the total populations.

$$\frac{\partial}{\partial t}N''_x(\theta) = -\frac{3}{h\nu_L}I_L\cos^2(\theta)\sigma_x(\nu_L)N''_x(\theta) + \sum_y \frac{N'_{x,y}}{\tau_{F,x,y}} - \frac{1}{\tau''_{0,x}}[N''_x(\theta) - N''_x] + \sum_w k''_{ex,x,w}N_{ex,x,w} \tag{9}$$

$$\frac{\partial}{\partial t}N'_{x,y}(\theta) = \frac{1}{h\nu_L}I_L[3\cos^2(\theta)\sigma_{x,y}(\nu_L)N''_x(\theta) - \sigma_{ex,x,y,w}N'_{x,y}(\theta)] - \frac{N'_{x,y}(\theta)}{\tau_{F,x,y}} - \frac{1}{\tau'_{0,x}}[N'_{x,y}(\theta) - N'_{x,y}]$$

$$+ \sum_w k'_{ex,x,y,w}N_{ex,x,w}. \tag{10}$$

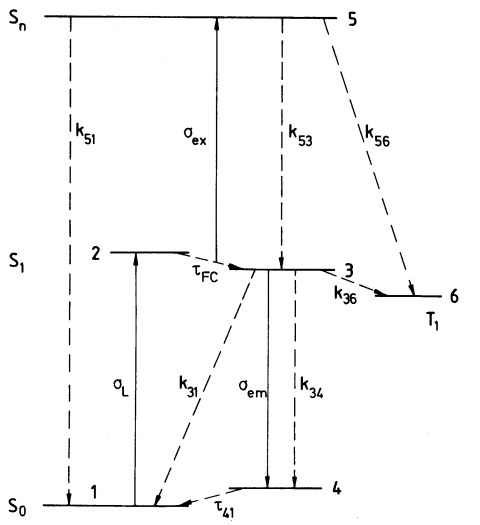

Figure 3 Six-level system for dye molecules with relevant transitions.

The above procedure shows that for the reasonable assumption of fast vibronic relaxation and cross-relaxation within an electronic band [53] the interaction of laser light with dye solution may be described by a simple level system as that shown in Fig. 3. In [54] the situation of finite cross-relaxation τ_s'' is discussed where the S_0-band is reduced to two levels. A similar two-level representation of the S_0-band is applied in fluorescence studies (Sections 3.1 and 3.2, levels 1 and 4 of Fig. 3). In Section 3.4 a finite relaxation time $\tau_{FC}(\tau_{v'} \neq 0$ or $\tau_s' \neq 0)$ out of the excited Franck–Condon states without their refilling is assumed, which results in two differential equations for the S_1-state population (levels 2 and 3 of Fig. 3).

3. Analysis of various S_1-state lifetime measurement techniques

The reduced model of interaction of laser light with dye solutions, developed in the previous section, is applied and extended to discuss various techniques of S_1-state lifetime measurements. For the sake of simplicity it is assumed in the following that all dye molecules are dissolved into monomers (low and medium dye concentrations).

3.1. Fluorescence measurements

The measurement of the $S_1 \rightarrow S_0$ fluorescence signal of dye solutions excited with picosecond pump pulses allows one to determine the S_1-state lifetime. The relaxation time constant is inferred from the time dependence of the fluorescence signal in the time range where the excitation pulse has already declined. The time resolution is limited by the steepness of the trailing part of the pump pulse. The S_1 state population decays by spontaneous emission, amplified spontaneous emission [55] (stimulated emission of fluorescence light) and radiationless relaxation.

A level system with the transitions involved is depicted in Fig. 3. A dye cell of length l is excited with a laser pulse of duration Δt_L and beam diameter d (radial coordinate r). The temporal development of the fluorescence signal in the forward direction $I_{F\parallel}$ and in the sideways direction $I_{F\perp}$ is analysed after the pump pulse has passed $(t' > t_0 \gtrsim 3\Delta t_L)$. In this time region the equation system for the fluorescence emission reads

$$\frac{\partial}{\partial t'} N_3(z', t') = -\frac{1}{h\nu_F} I_{F\parallel} N_3 \sigma_{em} - \frac{N_3}{\tau_F} \tag{11}$$

$$\frac{\partial I_{F\parallel}}{\partial z'} = I_{F\parallel} N_3 (\sigma_{em} - \sigma_{ex}) + \frac{h\nu_F q_F N_3 \Delta\Omega_{\parallel}}{4\pi\tau_F} \tag{12}$$

$$\frac{\partial I_{F\perp}}{\partial r} = \frac{h\nu_F q_F N_3 \Delta\Omega_{\perp}}{4\pi\tau_F} \tag{13}$$

The transformations $t' = t - (\eta/c_0)z$ and $z' = z$ are used. N_3 is the total population of the S_1-state $[N_3 = \int N'_{M,S_1}(\theta) \sin\theta \, d\theta$ using the notation of Section 2]. Polarization aspects [49, 50, 56] of the fluorescence light are neglected. σ_{em} is the isotopic stimulated emission cross-section. In Equation 11 the first term describes amplified spontaneous emission [50] while the second term comprises spontaneous emission and radiationless transitions. The spontaneous lifetime is $\tau_F = (k_{31} + k_{34} + k_{36})^{-1} = k_3^{-1}$ where k_{31} is the internal conversion rate, k_{34} is the radiative relaxation rate and k_{36} is the intersystem crossing rate. The fluorescence emission in the forward direction (Equation 12) is due to stimulated emission (first term) of present fluorescence light and due to spontaneous emission (second term). $q_F = \tau_F/\tau_{rad} = k_{34}/k_3$ is the fluorescence quantum yield. $\Delta\Omega_{\parallel} \simeq \pi d^2/(4l^2)$ is the solid angle of efficient amplified spontaneous emission. The fluorescence emission in the sideways direction (Equation 13) is only due to spontaneous emission. $\Delta\Omega_{\perp}$ is the solid angle of light picked up by the detection system in the sideways direction.

Integration of Equations 10–12 leads to

$$N_3(t', z') = N_3(t_0, z') \exp\left\{-\left[\frac{t' - t_0}{\tau_F} + \frac{\sigma_{em}}{h\nu_F}\int_{t_0}^{t'} I_{F\parallel}(t, z')dt\right]\right\} \tag{14}$$

$$I_{F\perp}(t', z') = \frac{h\nu_F q_F \Delta\Omega_\perp d}{4\pi\tau_F} N_3(t', z') \tag{15}$$

$$I_{F\parallel}(t', z') = \frac{h\nu_F q_F \Delta\Omega_\parallel}{4\pi\tau_F(\sigma_{em} - \sigma_{ex})} \{\exp[(\sigma_{em} - \sigma_{ex})N_3(\tilde{t}, \tilde{z})z'] - 1\}. \tag{16}$$

In Equation 16, $t_0 < \tilde{t} < t'$ and $0 < \tilde{z} < z'$. The sideways fluorescence signal (Equation 15) is proportional to the singlet state population N_3 and decays with the S_1-state lifetime $\tau_3(t')$:

$$\tau_3 = \left[\frac{1}{\tau_F} + \frac{\sigma_{em}}{h\nu_F(t' - t_0)} \int_{t_0}^{t'} I_{F\parallel}(t, z')\,dt\right]^{-1}. \tag{17}$$

To obtain the intrinsic small excitation S_1-state lifetime τ_F from the time resolved fluorescence signal $I_{F\perp}(t', z')$, it is necessary that $h\nu_F/I_{F\parallel}(t_0, z')\sigma_{em} \gg \tau_F$. Using Equation 16 this condition leads to

$$N_3(t_0, z') < \frac{1}{(\sigma_{em} - \sigma_{ex})z'} \ln\left[1 + \frac{4\pi(\sigma_{em} - \sigma_{ex})}{q_F \Delta\Omega_\parallel \sigma_{em}}\right]. \tag{18}$$

This condition is satisfied at sufficiently long delay times t_0. It is fulfilled for all delay times if Relation 18 holds for the total dye concentration N or the pump pulse intensity I_L is so small that $I_L \Delta t_L[1 - \exp(-\sigma_L N z')]/(h\nu_L z')$ remains small compared to the right-hand side of the inequality in Relation 18.

For a typical example with parameters $\sigma_L = \sigma_{em} = 3 \times 10^{-16}\,cm^2$, $\sigma_{ex} = 0$, $z' = 2\,cm$, $d = 2\,mm$, $q_F = 1$, $\Delta\Omega_\parallel = 10^{-2}\,sr$ and $\tilde{\nu}_L = \nu_L/c_0 = 14\,000\,cm^{-1}$ the condition in Relation 18 is fulfilled for $N < 10^{16}\,cm^{-3} \simeq 1.5 \times 10^{-5}\,mol\,l^{-1}$ or $I_L \Delta t_L < 7 \times 10^{-3}\,J\,cm^{-2}$ (see also Section 4.7).

The complication of the dependence of the sideways fluorescence emission on pump pulse polarization and molecular reorientation (not included in Equations 10–12) is avoided by observing the fluorescence behind a polarizer oriented at an angle of 54.7° to the polarization direction of the exciting laser pulse [57, 58, 52].

3.2. Fluorescence quantum yield measurements

Another technique of S_1-state lifetime measurement determines the fluorescence quantum yield. This technique is applicable for all pump pulse durations. The fluorescence quantum efficiency is defined using the notation of Fig. 3 as

$$q_F = \frac{k_{34}}{k_{31} + k_{34} + k_{36}} = \frac{\tau_F}{\tau_{rad}} \tag{19}$$

and the spontaneous S_1-state lifetime is

$$\tau_F = q_F \tau_{rad}. \tag{20}$$

$k_{34} = \tau_{rad}^{-1}$ is the radiative transition rate. k_{31} and k_{36} describe nonradiative transition rates. The quantum efficiency q_F is determined by the ratio of total emitted fluorescence photons to absorbed laser photons. A direct measurement of q_F is complicated. It is mostly determined by comparing the fluorescence emission of the test substance with a standard dye of known quantum efficiency [59]. The radiative lifetime τ_{rad} is calculated from the integrated absorption spectrum by quantum mechanical radiation theory [30]:

$$\tau_{rad}^{-1} = 8\pi\eta^2 c_0 \frac{\int I_F(\tilde{\nu})\tilde{\nu}^{-1}\,d\tilde{\nu}}{\int I_F(\tilde{\nu})\tilde{\nu}^{-4}\,d\tilde{\nu}} \int \sigma_L(\tilde{\nu})\tilde{\nu}^{-1}\,d\tilde{\nu} \tag{21}$$

The integration spans the S_1–S_0 fluorescence region (I_F) and the S_0–S_1 absorption range (σ_L).

3.3. Gain measurements

The population of the S_1-state may be measured with a picosecond pump and probe technique [31]. A picosecond pump pulse of frequency ν_L excites the molecules to the S_1-state. A time delayed weak

picosecond probe pulse of frequency ν_P in the region of the fluorescence band is amplified by the population of the S_1-state.

The probe pulse amplification at a delay time t_D is determined by the differential equation

$$\frac{\partial I_P}{\partial z'} = 3I_P[\sigma_{em}(\nu_P) - \sigma_{ex}(\nu_P)] \int_0^{\pi/2} N_3(t_D, z', \theta) \cos^2\theta \sin\theta \, d\theta. \tag{22}$$

The solution of this equation is

$$I_P(l) = I_P(0) \exp\left[3(\sigma_{em} - \sigma_{ex}) \int_0^l \int_0^{\pi/2} N_3(t_D, z', \theta) \cos^2\theta \sin\theta \, d\theta \, dz'\right] = I_P(0) \exp[G(t_D)]. \tag{23}$$

The gain of the probe pulse is

$$G(t_D) = \ln[I_P(l)/I_P(0)] = 3(\sigma_{em} - \sigma_{ex}) \int_0^l \int_0^{\pi/2} N_3(t_D, z, \theta) \cos^2\theta \sin\theta \, d\theta \, dz. \tag{24}$$

It has the same time dependence as the S_1-state population N_3 and the same constraints apply to the determination of the S_1-state lifetime τ_F as discussed in Section 3.1. The problems of absorption anisotropy and molecular reorientation can be avoided by applying linear polarized pump and probe pulses wih an angle of 54.7° between the polarization directions [52].

3.4. Absorption recovery of probe pulse

With intense picosecond pump pulses the ground state population may be reduced considerably by promoting molecules to the S_1-state. The absorption of a weak time delayed picosecond probe pulse of frequency $\nu_p \geqslant \nu_L$ is reduced and recovers to the initial absorption as the delay time is increased and the molecules return to the ground state [16, 32–35]. The technique is only applicable for relaxation times τ_F long compared to the duration of the pump pulse and the interrogating probe pulse ($\tau_F \gtrsim 3\Delta t_L$). Otherwise the molecules have returned to the ground state before the probe pulse is delayed long enough not to interfere with the pump pulse. The technique is often applied in the analysis of fast laser dyes and saturable absorbers [16, 32–35, 60–62].

The absorption of a probe pulse I_P of polarization direction at an angle of 54.7° to the polarization of the pump pulse at delay time t_D is governed by the equation

$$\frac{\partial}{\partial z'} I_P = -I_P\{\sigma_P[N - N_3(t_D, z')] + \sigma_{ex} N_3(t_D, z')\}. \tag{25}$$

$N - N_3(t_D) = N_1(t_D)$ is the population of the ground state S_0 at delay time t_D. The triplet state population is neglected.

The transmitted probe pulse intensity through a sample of length l is

$$I_P(l) = I_P(0) \exp\left[-\sigma_P N l + (\sigma_P - \sigma_{ex}) \int_0^l N_3(t_D, z) \, dz\right] = I_P(0) \exp[-L(t_D)]. \tag{26}$$

The loss $L(t_D) = \ln[I_P(0)/I_P(l)]$ of the probe pulse at delay time t_D is

$$L(t_D) = -\ln[T(t_D)] = -\ln(T_0) - (\sigma_P - \sigma_{ex}) \int_0^l N_3(t_D, z) \, dz. \tag{27}$$

$T = I_P(l)/I_P(0)$ is the intensity transmission and $T_0 = \exp(-\sigma_P N l)$ the initial transmission (no excitation) of the probe pulse. The loss L relaxes in the same manner as $N_3(t_D)$. If the condition in Relation 18 is satisfied $L(t_D)$ relaxes exponentially with the S_1-state lifetime τ_F as does $N_3(t_D)$. It was shown above that this condition is fulfilled for $Nl < 2 \times 10^{16}\,\mathrm{cm}^{-2}$ or $T_0 = \exp(-N\sigma_P l) > 10^{-4}$ ($\sigma_P \simeq 3 \times 10^{-16}\,\mathrm{cm}^2$).

3.5. Single pulse bleaching

The bleaching of the pump pulse itself may be employed to calculate the lifetime of molecules excited to the S_1-state [36–42, 63]. If the relaxation time τ_F is comparable to or shorter than the pump pulse duration ($\tau_F \lesssim \Delta t_L$) the transmission of the pump pulse at a fixed peak intensity depends on the ratio $\Delta t_L/\tau_F$ which indicates how often the molecules return to the ground state within the excitation pulse duration. Using picosecond pump pulses the technique is applicable to dyes with picosecond recovery times. Such dyes are frequently used as saturable absorbers [2].

The dye level scheme of Fig. 3 is used to describe the interaction of a single picosecond pump pulse with the absorber. Amplified spontaneous emission is not included in the following equation system, Equations 28–36, since experimental conditions may be arranged so that it is negligible [46, 59] (see Section 4.7). The ground state S_0 is described by only a single level 1. The rate $k_{S_1S_0} = k_{31} + k_{34}$ is the total transfer rate from S_1 to S_0 and the spontaneous S_1-state lifetime is $\tau_F = (k_{S_1S_0} + k_{36})^{-1}$. The differential equation system for pump pulse propagation and population dynamics is

$$\frac{\partial I_L}{\partial z'} = -I_L \int_0^{\pi/2} \{3\sigma_L \cos^2(\theta)[N_1(\theta) - N_2(\theta)] + \sigma_{ex}[N_2(\theta) + N_3(\theta)] - 3\sigma_{eL} \cos^2(\theta) N_3(\theta)\} \sin\theta \, d\theta \tag{28}$$

$$\frac{\partial}{\partial t'} N_1(\theta) = -\frac{3I_L}{h\nu_L} \cos^2(\theta)\{\sigma_L[N_1(\theta) - N_2(\theta)] - \sigma_{eL} N_3(\theta)\} + k_{S_1S_0}[(N_2(\theta) + N_3(\theta)] + k_{51} N_5(\theta)$$

$$-\frac{1}{\tau_0''}[N_1(\theta) - N_1] + k_{61} N_6 \tag{29}$$

$$\frac{\partial}{\partial t'} N_2(\theta) = \frac{I_L}{h\nu_L}\{3\sigma_L \cos^2(\theta)[N_1(\theta) - N_2(\theta)] - \sigma_{ex}[N_2(\theta) - N_5(\theta)]\} - \left(\frac{1}{\tau_{FC}} + k_{S_1S_0}\right) N_2(\theta)$$

$$-\frac{1}{\tau_0'}[N_2(\theta) - N_2] \tag{30}$$

$$\frac{\partial}{\partial t'} N_3(\theta) = -\frac{I_L}{h\nu_L}\{\sigma_{ex}[N_3(\theta) - N_5(\theta)] + 3\sigma_{eL} \cos^2(\theta) N_3(\theta)\} + \frac{1}{\tau_{FC}} N_2(\theta) + k_{53} N_5(\theta)$$

$$-(k_{S_1S_0} + k_{36}) N_3(\theta) - \frac{1}{\tau_0'}[N_3(\theta) - N_3] \tag{31}$$

$$\frac{\partial}{\partial t'} N_5(\theta) = \frac{I_L}{h\nu_L} \sigma_{ex}[N_2(\theta) + N_3(\theta) - N_5(\theta)] - \frac{1}{\tau_{ex}} N_5(\theta) \tag{32}$$

$$\frac{\partial}{\partial t'} N_6 = k_{36}(N_3 + N_2) + k_{56} N_5 - k_{61} N_6. \tag{33}$$

The higher excited state lifetime is $\tau_{ex} = (k_{53} + k_{51} + k_{56})^{-1} = k_5^{-1}$. The initial conditions are

$$N_1(r, z', t' = -\infty, \theta) = N \tag{34}$$

$$N_2(r, z', t' = -\infty, \theta) = N_3(r, z', t' = -\infty, \theta) = N_5(r, z', t' = -\infty, \theta) = N_6(r, z', t' = -\infty) = 0 \tag{35}$$

$$I_L(r, z' = 0, t') = I_{OL} s(r) s'(t'). \tag{36}$$

A rotational symmetric beam profile for the laser is assumed [$s(x, y) = s(r)$]. I_{OL} is the input peak intensity of the laser pulse.

In contrast to the procedure leading to Equations 9 and 10 the condition of infinitely fast relaxation $\tau_{v'} = 0$ and $\tau_s' = 0$ out of the excited Franck–Condon levels is softened to a finite lifetime τ_{FC} which leads to a two-level description of the S_1-band and the presence of the two rate Equations 30 and 31.

The stimulated emission cross-section σ_{eL} for the interaction of molecules in level 3 with laser light is about zero, if the laser frequency ν_L is equal to or greater than the frequency ν_{max} of maximum S_0–S_1 absorption (no stimulated transition from level 3 to the ground state at frequency $\nu_L \geqslant \nu_{max}$). The situation changes if $\nu_L < \nu_{max}$, i.e. when ν_L lies at the long-wavelength side of the absorption band (the fluorescence region) [64]. This case is discussed in [54]. The relaxation of the higher lying singlet states S_n (level 5) populated by excited-state absorption may proceed to the S_1-state (rate k_{53}) to the ground state (rate k_{51}) and to the triplet system (rate k_{56}).

The rate equation system (Equations 28–33) has to be solved numerically. A comparison of the experimentally measured pure energy transmission $T_E = W_L(l)/W_L(0)$ ($W_L(l)$ is the transmitted pulse energy, $W_L(0)$ the incident pulse energy, reflection losses are not included in $W_L(l)$) with the calculations allows us to derive a value for the S_1-state lifetime τ_F. The energy transmission is obtained from the intensity values by means of the following expression

$$T_E = \frac{\int_0^\infty \int_{-\infty}^\infty rI_L(r,l,t')\,dt'\,dr}{I_{OL}\int_0^\infty \int_{-\infty}^\infty rs(r)s'(t')\,dt'\,dr} = \frac{\int_0^\infty \int_{-\infty}^\infty T[I_{OL}s'(r)s(t')]rs(r)s'(t')\,dt'\,dr}{\int_0^\infty \int_{-\infty}^\infty rs(r)s'(t')\,dt'\,dr}. \quad (37)$$

$T = I_L(l)/I_L(0)$ is the pure intensity transmission (without reflection losses).

In the following section numerical results of the dependence of T_E on pump and dye parameters are presented. The possibilities of model simplifications are discussed.

4. Influence of various parameters on single pulse bleaching

The influence of various pulse and dye parameters on the energy transmission is discussed. A set of parameters is selected that is responsible for a recent experiment of bleaching the saturable absorber DDI (1,1′-diethyl-2,2′-dicarbocyanine iodide) dissolved in methanol with picosecond ruby laser pulses [63]. These parameters are listed in Table I. Single parameters are varied to analyse their particular influence on the bleaching and their relevance to the measurement of the S_1-state lifetime τ_F.

TABLE I Selected pulse and dye parameters

Laser	
Spatial shape:	Gaussian $s(r) = \exp[-(r/r_0)^2]$
Temporal shape:	Gaussian $s'(t) = \exp[-(t/t_0)^2]$
Pulse duration (FWHM):	$\Delta t_L = 25$ ps
Frequency (ruby laser):	$\bar{\nu}_L = \nu_L/c = 14\,403\ \mathrm{cm}^{-1}$
Dye	
Isotropic ground state absorption cross-section	$\sigma_L = 7.6 \times 10^{-16}\ \mathrm{cm}^2$
Effective isotropic excited state absorption cross-section:	$\sigma_{ex} = 0$
Emission cross-section at ν_L from level 3 (Fig. 3):	$\sigma_{eL} = 0$
Intrinsic S_1-state lifetime:	$\tau_F = 15$ ps
S_1–T_1 intersystem crossing rate:	$k_{36} = 0$
S_n–S_1 decay rate:	$k_{53} = 10^{13}\ \mathrm{s}^{-1}$
S_n–S_0 decay rate:	$k_{51} = 0$
S_n–T_1 decay rate:	$k_{56} = 0$
T_1–S_0 decay rate:	$k_{61} = 0$
Franck–Condon state lifetime in S_1:	$\tau_{FC} = 1$ ps
Relaxation time in S_0:	$\tau_{41} = 0$
Reorientation time in S_0:	$\tau_0'' = 100$ ps
Reorientation time in S_1:	$\tau_0' = 100$ ps
Concentration:	$c = 3.82 \times 10^{-6}\ \mathrm{mol\,l}^{-1}$, $N = 2.3 \times 10^{15}\ \mathrm{cm}^{-3}$
Sample length:	$l = 2$ cm

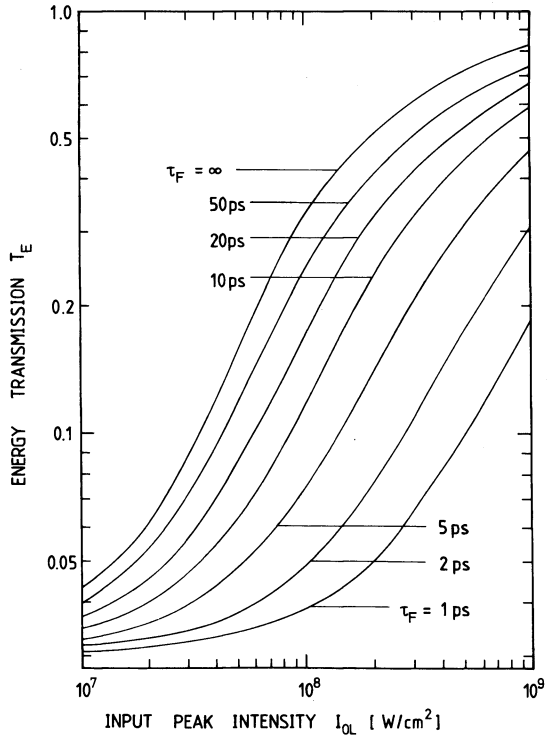

Figure 4 Energy transmission versus input peak laser intensity for various S_1-state lifetimes τ_F. Duration of excitation pulse $\Delta t_L = 25$ ps. Further parameters are listed in Table I.

4.1. S_1-state lifetime τ_F

The intensity-dependent bleaching of the pump pulse is used to determine the S_1-state lifetime τ_F. For the pump and dye parameters listed in Table I the energy transmission T_E versus input peak intensity I_{OL} is plotted in Fig. 4 ($\Delta t_L = 25$ ps). The Equation system 28–37 is used in the calculations. τ_F is varied between ∞ and 1 ps. For $\tau_F > 2\Delta t_L$ (transient regime) the energy transmission becomes practically independent of relaxation time τ_F at a fixed pump pulse intensity I_{OL}, i.e. τ_F cannot be determined from single pulse bleaching experiments for $\tau_F > 2\Delta t_L$. For $\tau_F \leqslant \Delta t_L$ (intermediate and stationary regime), T_E reduces significantly with decreasing τ_F and the S_1-state lifetime is easily determined from a measurement of $T_E(I_{OL})$. The pump intensity necessary to reach a certain transmission value is approximately proportional to the relaxation rate $\tau_F^{-1} = k_{S_1S_0}$ as is indicated in Fig. 5 for $T_E = 0.05$, 0.15 and 0.25 (intersystem crossing rate $k_{36} = 0$ is assumed). The intercepts on the ordinate axis are determined by the number of laser photons necessary to excite dye molecules once to the S_1-state without returning to the ground state (absorbed photons = excited molecules for $\tau_F \to \infty$). The position of $\tau_F = \Delta t_L$ is indicated. Fig. 5 reveals clearly that τ_F can be determined only for $\tau_F \leqslant \Delta t_L$.

4.2. Temporal and spatial pulse shape

Fig. 6 presents the dependence of the energy transmission $T_E(I_{OL})$ on the temporal pulse shape. A Gaussian spatial shape is assumed. Curves are shown for Lorentzian (1), hyperbolic secant (2), Gaussian (3) and rectangular (4) shapes. The energy transmission varies only slightly with pulse shape. Experimentally, an asymmetric pulse shape with a Gaussian rising part and a hyperbolic secant decaying part is observed [65, 66]. The energy transmission for this shape lies between the Gaussian and the hyperbolic secant shape and is well represented by one of these profiles.

In Fig. 7 the energy transmission versus input peak intensity is depicted for a rectangular shape (1), a TEM_{01}-mode (2), a Gaussian shape (TEM_{00}-mode, curve 3), and the diffraction pattern of a circular aper-

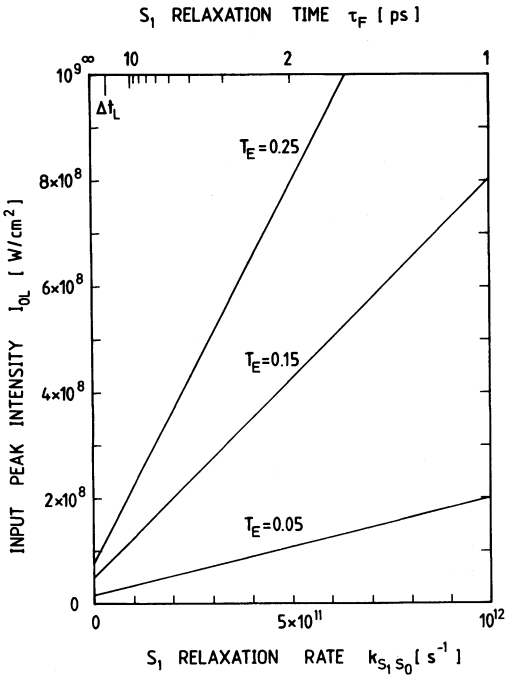

Figure 5 Input laser peak intensity versus S_1-state lifetime τ_F for various energy transmissions T_E. Pump pulse duration $\Delta t_L = 25$ ps. Parameters are listed in Table I.

ture (4). The influence of the pulse shape on the energy transmission at a fixed input peak intensity cannot be neglected. For example, at $I_{OL} = 10^8\,W\,cm^{-2}$ the energy transmission is $T_E = 0.14$ for a Gaussian profile and $T_E = 0.32$ for a rectangular distribution. At a fixed transmission T_E the input peak intensity I_{OL} for a Gaussian shape is about a factor of two larger than for a rectangular distribution. Energy trans-

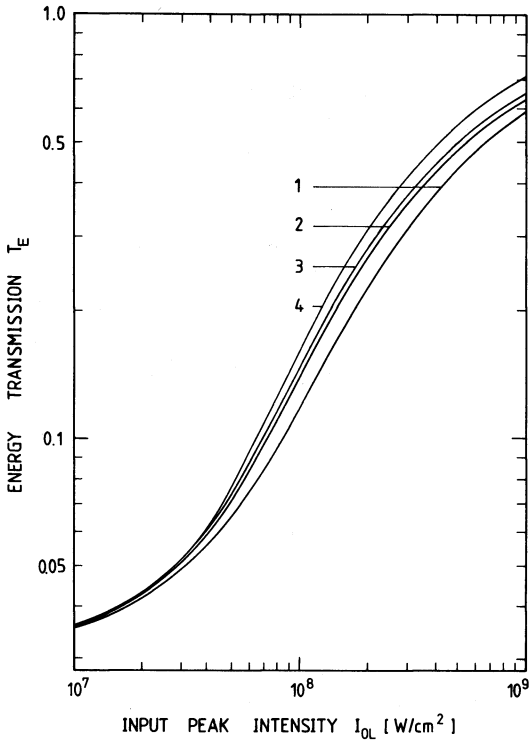

Figure 6 Influence of temporal pulse shape on energy transmission versus input pulse peak intensity. Spatial shape is Gaussian. Parameters are listed in Table I. Curves: 1, Lorentzian $s'(t') = [1 + (2t'/\Delta t_L)^2]^{-1}$; 2, hyperbolic secant $s'(t') = [\cosh^2(1.76274t'/\Delta t_L)]^{-1}$; 3, Gaussian $s'(t') = \exp[-4(\ln 2)t'^2/\Delta t_L^2]$; 4, rectangular $s'(t') = \theta(t' + \Delta t_L/2) - \theta(t' - \Delta t_L/2)$.

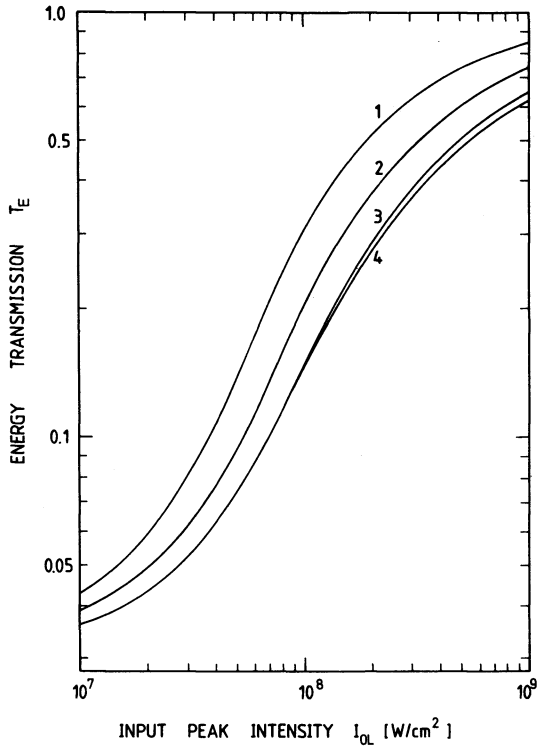

Figure 7 Influence of spatial pulse shape on energy transmission versus input laser peak intensity. Temporal shape is Gaussian. Parameters are listed in Table I. Curves: 1, rectangular $s(r') = 1$; 2, TEM_{01}-mode $s(r') = r'^2 \exp[-(1-r')^2]$; 3, Gaussian $s(r') = \exp(-r'^2)$; 4, diffraction pattern of circular aperture $s(r') = [2J_1(r')/r']^2$ truncated at second zero position, $J_1(r')$ is the Bessel function. The result is independent of laser pulse diameter.

mission calculations with a pulse shape approximating the experimental shape are necessary for an accurate determination of the S_1-state lifetime.

4.3. Molecular reorientation τ_0

The molecular reorientation of photoselected molecules depends on the molecular size and the solvent viscosity (for reviews see [58, 67]). Its influence on single pulse bleaching is plotted in Fig. 8. Equal reorientation times in the ground state and S_1-state are assumed ($\tau_0 = \tau_0'' = \tau_0'$). For $\tau_0 \gtrsim 2\tau_F$ the molecular reorientation may be neglected and the anisotropic molecular distribution generated by electric dipole interaction governs the bleaching. If $\tau_0 \lesssim \tau_F/10$ the isotropic absorption regime is approached ($\tau_0 \to 0$). Fig. 8 indicates that at $T_E = 0.1$ the corresponding input peak laser intensities are $I_{OL} = 7 \times 10^7 \mathrm{W\,cm^{-2}}$ for $\tau_0 = \infty$ (anisotropic case) and $I_{OL} = 1.2 \times 10^8 \mathrm{W\,cm^{-2}}$ for $\tau_0 = 0$ (isotropic case). In the range $2\tau_F > \tau_0 > \tau_F/10$ the molecular reorientation has to be included in the calculations. If $\tau_0 > 2\tau_F$, the reorientation time may be set to $\tau_0 = \infty$. In the case of $\tau_0 < \tau_F/10$ the isotropic problem may be calculated, where Equations 28–32 reduce to:

$$\frac{\partial I_L}{\partial z'} = -I_L[\sigma_L(N_1 - N_2) + \sigma_{ex}(N_2 + N_3) - \sigma_{eL}N_3] \tag{38}$$

$$\frac{\partial}{\partial t'}N_1 = -\frac{I_L}{h\nu_L}[\sigma_L(N_1 - N_2) - \sigma_{eL}N_3] + \frac{1}{\tau_F}(N_2 + N_3) + k_{51}N_5 + k_{61}N_6 \tag{39}$$

$$\frac{\partial}{\partial t'}N_2 = \frac{I_L}{h\nu_L}[\sigma_L(N_1 - N_2) - \sigma_{ex}(N_2 - N_5)] - \left(\frac{1}{\tau_{FC}} + k_{S_1S_0}\right)N_2 \tag{40}$$

$$\frac{\partial}{\partial t'}N_3 = -\frac{I_L}{h\nu_L}[\sigma_{ex}(N_3 - N_5) + \sigma_{eL}N_3] + \left(\frac{1}{\tau_{FC}} - k_{S_1S_0} - k_{36}\right)N_3 + k_{53}N_5 \tag{41}$$

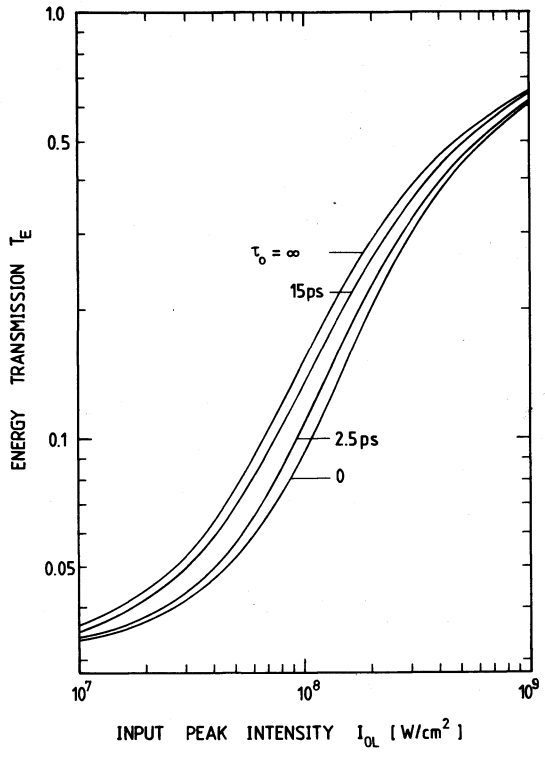

Figure 8 Dependence of energy transmission on molecular reorientation time. An equal reorientation time τ_0 in the ground state and the excited state is assumed. Pulse duration $\Delta t_L = 25$ ps, S_1-state lifetime $\tau_F = 15$ ps.

$$\frac{\partial}{\partial t'} N_5 = \frac{I_L}{h\nu_L} \sigma_{ex}(N_2 + N_3 - N_5) - \frac{1}{\tau_{ex}} N_5 \tag{42}$$

with $N_i = \int_0^{\pi/2} N_i(\theta) \sin\theta \, d\theta$, $i = 1$–6. Equation 33 remains unchanged.

4.4. Franck–Condon relaxation time τ_{FC}

The influence of τ_{FC} on $T_E(I_{OL})$ is shown in Fig. 9. The limiting cases of $\tau_{FC} = \infty$ (no relaxation out of the Franck–Condon state within the S_1-state lifetime), $\tau_{FC} = 0$ (instantaneous relaxation) and the intermediate cases $\tau_{FC} = \tau_F$ and $\tau_{FC} = \tau_F/6$ are plotted. In the case of $\tau_{FC} = \infty$ only half the molecules in the ground state can be excited, since for $N_1 = N_2$ it follows that $T_E = 1$ (two-level system). For $\tau_{FC} = 0$ all the molecules may be excited to the S_1-state at high pump pulse intensities (three-level system with fast intermediate state decay). The intensity necessary to reach a fixed energy transmission T_E is about a factor of two higher for $\tau_{FC} = 0$ than for $\tau_{FC} = \infty$. For $\tau_{FC} > 2\tau_F$ and $\tau_{FC} < \tau_F/10$ the limiting cases may be used as good approximations. Experimentally, relaxation times $\tau_{FC} \leqslant 1$ ps have been observed [64, 68, 69].

4.5. Excited state absorption σ_{ex}

The excited state absorption cross-section σ_{ex} is varied in Fig. 10. The excited state absorption limits the final transmission at high input intensities. If $\sigma_{ex} > \sigma_L$ no increase of energy transmission but a decrease of T_E with I_{OL} occurs. Fitting the measured energy transmission at high pump pulse intensities allows one to determine σ_{ex} by bleaching experiments. The S_1-state lifetime τ_F governs the energy transmission at lower pulse intensities. Both parameters τ_F and σ_{ex} may be determined by fitting a measured $T_E(I_{OL})$-curve. For DDI a value of $\sigma_{ex} \simeq 5 \times 10^{-17}$ cm^2 was found in [63]. As σ_{ex} increases the accuracy of the τ_F determination is reduced. If σ_{ex} becomes comparable to σ_L, then τ_F can no longer be determined by $T_E(I_{OL})$ measurements.

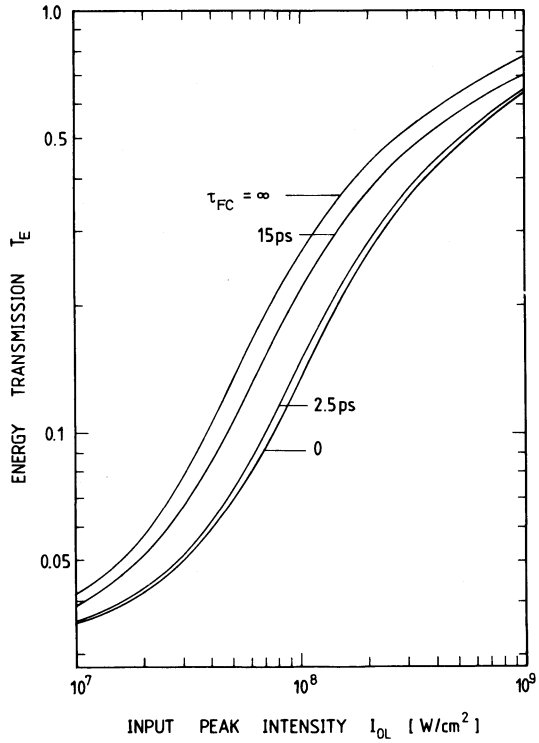

Figure 9 Dependence of energy transmission on Franck–Condon state relaxation time τ_{FC} in the S_1-band. Pulse duration $\Delta t_L = 25$ ps, S_1-state lifetime $\tau_F = 15$ ps.

4.6. Excited state relaxation τ_{ex}

The excited state relaxation is generally very fast, i.e. of the order of 10^{-13} s [56, 70]. The relaxation mainly terminates in the S_1-level. In Fig. 10 the dashed curve (a) represents the energy transmission T_E versus input peak intensity I_{OL} for $k_5 = k_{53} = 10^{11}\,s^{-1}$ and $\sigma_{ex}/\sigma_L = 0.1$ (return to the S_1-state, $\sigma_L = 7.6 \times 10^{-16}\,cm^2$). The solid curves are calculated for $k_5 = k_{53} = 10^{13}\,s^{-1}$. The dashed curve (b) is responsible for $k_5 = k_{51} = 10^{13}\,s^{-1}$ and $\sigma_{ex}/\sigma_L = 0.1$ (return to the ground state). The influence of k_{53} and k_{51} on energy transmission is very small for reasonable values of σ_{ex} and τ_{ex}. The influence of transitions to the triplet state k_{56} will be discussed later.

4.7. Amplified spontaneous emission

To discuss the influence of amplified spontaneous emission the differential Equation system 28–33 has to be extended to include the build up of fluorescence light [50] (transition from level 3 to 4 in Fig. 3). This problem was treated in Section 3.1. The S_1-state lifetime τ_3 is given by Equation 17. Insertion of Equation 16 into Equation 17 gives

$$\tau_3 = \frac{\tau_F}{1 + \dfrac{q_F \Delta\Omega_{\parallel} \sigma_{em}}{4\pi(\sigma_{em} - \sigma_{ex})} \{\exp[(\sigma_{em} - \sigma_{ex}) N_3(\bar{t}, \bar{z}) l] - 1\}} \tag{43}$$

with $-\infty < \bar{t} < \infty$ and $0 < \bar{z} < l$. Reasonable values of $\bar{t}$ and $\bar{z}$ are $\bar{t} = 0$ and $\bar{z} = l/2$. Upper and lower limits of τ_3/τ_F are derived from Equation 43 by using the relation $0 \leqslant N_3(\bar{t}, \bar{z}) \leqslant N$ and the initial transmission $T_0 = \exp[-\sigma_L N l]$.

$$1 \geqslant \frac{\tau_3}{\tau_F} \geqslant r_\tau = \frac{1}{1 + \dfrac{q_F \Delta\Omega_{\parallel} \sigma_{em}}{4\pi(\sigma_{em} - \sigma_{ex})} \left[T_0^{-\left(\frac{\sigma_{em} - \sigma_{ex}}{\sigma_L}\right)} - 1 \right]}. \tag{44}$$

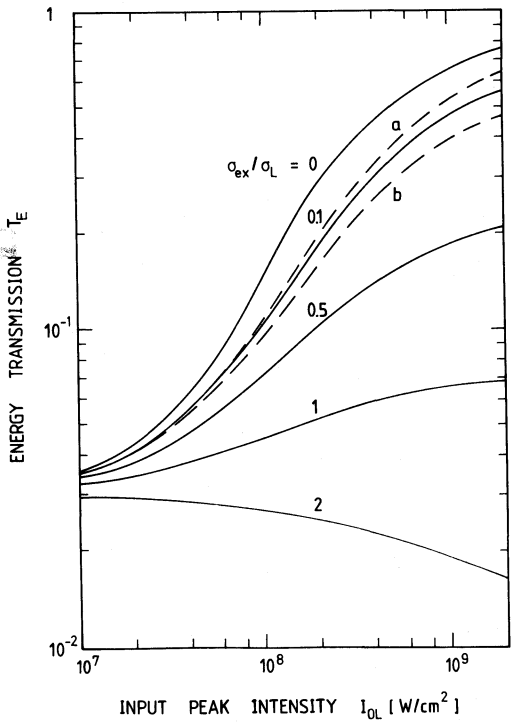

Figure 10 Energy transmission T_E as a function of input peak laser intensity. Excited state absorption cross-section is varied. Other parameters are listed in Table I. Solid curves: S_n-relaxation rate $k_5 = k_{53} = 10^{13}\,s^{-1}$. Dashed curves: a, $k_5 = k_{53} = 10^{11}\,s^{-1}$ and $\sigma_{ex}/\sigma_L = 0.1$; b, $k_5 = k_{51} = 10^{13}\,s^{-1}$ and $\sigma_{ex}/\sigma_L = 0.1$.

Relation 44 may be used to determine the lowest initial transmission T_0 for which τ_3 remains still nearly equal to the spontaneous S_1-state lifetime τ_F and the Equation system 28–33 is correct.

Fig. 11 shows the dependence of the lower limit r_τ of τ_3/τ_F versus T_0 for the values of $q_F = 10^{-3}$ (saturable absorbers), $\Delta\Omega_{||} = 10^{-2}$ sr ($d = 2$ mm, $l = 2$ cm), $\sigma_{ex} = 0$, $\sigma_{em}/\sigma_L = 1$ (curve 1) and $\sigma_{em}/\sigma_L = 2$ (curve 2). The dashed curve 3 is calculated for a quantum efficiency $q_F = 1$ (laser dye) and $\sigma_{em}/\sigma_L = 1$ (other parameters unchanged). The curves indicate up to what initial transmission T_0 the shortening of the S_1-state lifetime by amplified spontaneous emission is negligibly small. For the parameters relevant to curve 1 one finds $1 > \tau_3/\tau_F > 0.9$ for $T_0 > 10^{-5}$.

r_τ depends strongly on the ratio $(\sigma_{em} - \sigma_{ex})/\sigma_L$ or σ_{em}/σ_L for $\sigma_{ex} = 0$. This ratio depends on the excitation frequency ν_L. In the case of excitation to the absorption maximum $\sigma_L = \sigma_{max}$ we have $\sigma_{em}/\sigma_L \simeq 1$. If the laser causes a transition in the wings of the absorption band we have $\sigma_{em}/\sigma_L \simeq \sigma_{max}/\sigma_L > 1$ and only small dye absorptions are allowed in order to avoid severe amplified spontaneous emission. Excitation in the fluorescence band of the dye (long-wavelength wing of the S_0–S_1 absorption band) causes additionally the amplification of input laser light by molecules in the S_1-state (term $\sigma_{eL}N_3$ in Equations 28–31) and intricates the S_1-state lifetime measurement. This problem is analysed in [54].

4.8. Intersystem crossing

Intersystem crossing from the singlet to the triplet state system reduces the number of molecules involved in singlet state absorption and causes triplet state transitions. A determination of τ_F from absorption recovery and single pulse bleaching experiments becomes practically impossible if the intersystem crossing rate becomes comparable to the S_1–S_0 relaxation time.

In the following the population of the triplet state (level 6 in Fig. 3) by intersystem crossing from the S_1-state (level 3) and from higher lying singlet states S_n (level 5) is estimated. A simplified equation system for the population of levels 3, 5 and 6 is applied (derived from Equations 33 and 39–40 with $\tau_{FC} = 0, N_1 \simeq N - N_3, k_{61} = 0$):

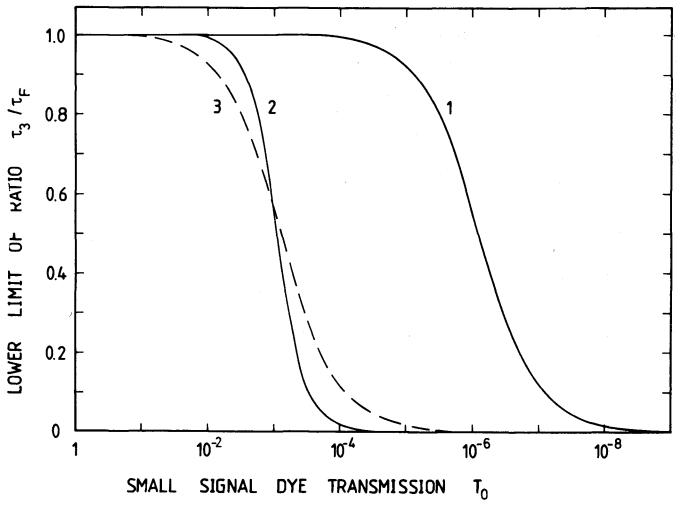

Figure 11 Effect of amplified spontaneous emission on the S_1-state lifetime τ_3. The lower limit of τ_3/τ_F versus the small signal dye transmission T_0 is presented (upper limit: $\tau_3/\tau_F = 1$). Curve 1: ratio of cross-sections $\sigma_{em}/\sigma_L = 1$, fluorescence quantum efficiency $q_F = 10^{-3}$, solid angle of amplified spontaneous emission $\Delta\Omega_{||} = 10^{-2}$ sr. Curve 2: $\sigma_{em}/\sigma_L = 2$, $q_F = 10^{-3}$, $\Delta\Omega_{||} = 10^{-2}$ sr. Curve 3: $\sigma_{em}/\sigma_L = 1$, $q_F = 1$, $\Delta\Omega_{||} = 10^{-2}$ sr.

$$\frac{\partial}{\partial t'} N_3 = \frac{I_L \sigma_L}{h\nu_L}(N - N_3) - \frac{N_3}{\tau_F} \tag{45}$$

$$\frac{\partial}{\partial t'} N_5 = \frac{I_L \sigma_{ex}}{h\nu_L} N_3 - \frac{N_5}{\tau_{ex}} \tag{46}$$

$$\frac{\partial}{\partial t'} N_6 = k_{36} N_3 + k_{56} N_5 \,. \tag{47}$$

These equations are solvable analytically. Assuming a rectangular temporal pulse shape of duration $\Delta t_L\{I_L(t) = I_{LO}[\theta(t) - \theta(t - \Delta t_L)]\}$ the solution of Equation 45 is

$$N_3(t' \leqslant \Delta t_L) = N \frac{I_L \sigma_L}{h\nu_L} \tau_A [1 - \exp(-t'/\tau_A)] \tag{48a}$$

and

$$N_3(t' > \Delta t_L) = N_3(\Delta t_L) \exp[-(t' - \Delta t_L)/\tau_F]. \tag{48b}$$

The abbreviation

$$\tau_A = \left(\frac{I_L \sigma_L}{h\nu_L} + \frac{1}{\tau_F}\right)^{-1}$$

is used.

Insertion of Equations 48a and b into Equation 46 leads to

$$N_5(t' \leqslant \Delta t_L) = N\sigma_L\sigma_{ex}\left(\frac{I_L}{h\nu_L}\right)^2 \tau_A\{\tau_{ex}[1 - \exp(-t'/\tau_{ex})] + \tau_B[\exp(-t'/\tau_{ex}) - \exp(-t'/\tau_A)]\} \tag{49a}$$

$$N_5(t' > \Delta t_L) = N_5(\Delta t_L) \exp[-(t' - \Delta t_L)/\tau_{ex}] \tag{49b}$$

where

$$\tau_B = \left(\frac{1}{\tau_{ex}} - \frac{1}{\tau_A}\right)^{-1}.$$

Integration of Equation 47 and using Equations 48 and 49 gives the triplet state population

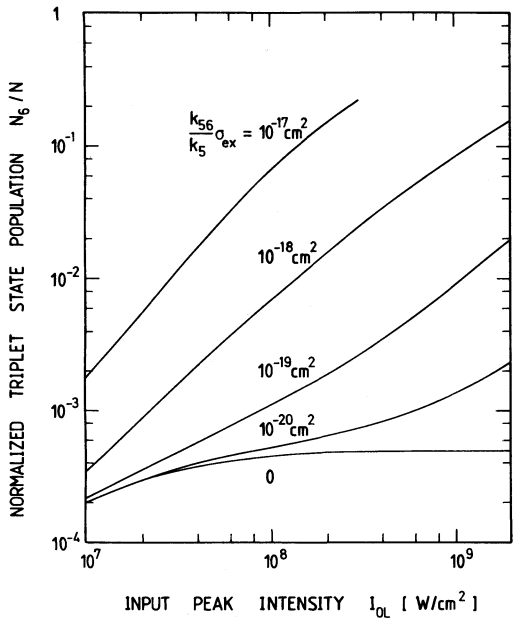

Figure 12 Triplet state population at end of excitation pulse versus input pulse intensity for various intersystem crossing rates. A rectangular temporal and spatial pulse shape is assumed. S_n-state relaxation rate $k_5 = \tau_{ex}^{-1} = 10^{13}\,s^{-1}$. S_1–T_1 intersystem crossing rate $k_{36} = 2 \times 10^7\,s^{-1}$. Curves present various products of excited state absorption σ_{ex} and branching ratio k_{56}/k_5.

$$N_6(t' \leqslant \Delta t_L) = N\frac{I_L\sigma_{OL}}{h\nu_L}\tau_A k_{36}\{t' - \tau_A[1-\exp(-t'/\tau_A)]\} + N\sigma_L\sigma_{ex}\left(\frac{I_L}{h\nu_L}\right)^2\tau_A k_{56}\tau_{ex}\left(\{t' - \tau_{ex}[1-\exp(-t'/\tau_{ex})]\} + \tau_B\left\{[1-\exp(-t'/\tau_{ex})] - \frac{\tau_A}{\tau_{ex}}[1-\exp(-t'/\tau_A)]\right\}\right) \quad (50a)$$

$$N_6(t > \Delta t_L) = N_6(\Delta t_L) + N_3(\Delta t_L)\tau_F\{1-\exp[-(t'-\Delta t_L)/\tau_F]\} + N_5(\Delta t_L)\tau_{ex}\{1-\exp[-(t'-\Delta t_L)/\tau_{ex}]\}. \quad (50b)$$

In Fig. 12 the ratio of triplet state population to total dye concentration N_6/N is plotted versus input peak intensity I_{OL} at $t' = \Delta t_L$ for the standard parameters of Table I (rectangular temporal and spatial pulse shape assumed). The S_1–T_1 rate constant is chosen to be $k_{35} = 2 \times 10^7\,s^{-1}$ (upper value for DDI in methanol [71, 72]). Curves are shown for various excited state absorptions σ_{ex} and branching ratios $k_{56}/(k_{51} + k_{53} + k_{56}) = k_{56}/k_5 = k_{56}\tau_{ex}$ ($N_6/N \propto \sigma_{ex}\, k_{56}/k_5$). Without excited state absorption we have $N_6(\Delta t_L)/N < k_{36}\Delta t_L$, which is negligible since the S_1–T_1 intersystem crossing rate k_{36} is small compared to Δt_L^{-1}. If the excited state absorption is remarkable, the triplet state population may become large at high pump pulse intensities. The branching ratio $k_{56}/k_5 = k_{56}\tau_{ex}$ determines the triplet state population. An estimate of the triplet state population has to be performed for any singlet state lifetime measurement by ground state bleaching (e.g. the recovery to initial ground state transmission after passage of pump pulse has to be probed). $N_6/N < 0.1$ may be tolerated. For high triplet state populations the determination of τ_F from T_E measurements becomes inaccurate and finally impossible.

5. Comparison with simple models

In the literature simple isotropic steady state models are often used to determine τ_F from single pulse transmission measurements [41, 42]. The most common isotropic two-level and three-level models [36–39, 73] are compared here with a more rigorous analysis.

5.1. Steady state isotropic two-level system

The equation system for an isotropic two-level system (states 1 and 2 of Fig. 3) reads

$$\frac{\partial I_L}{\partial z'} = -I_L \sigma_L (N_1 - N_2) \tag{51}$$

$$\frac{\partial N_1}{\partial t'} = -\frac{I_L \sigma_L}{h\nu_L}(N_1 - N_2) + \frac{N_2}{\tau_F} \tag{52}$$

$$\frac{\partial N_2}{\partial t'} = \frac{I_L \sigma_L}{h\nu_L}(N_1 - N_2) - \frac{N_2}{\tau_F}. \tag{53}$$

In the steady state $\tau_F \ll \Delta t_L$, the temporal variation of N_1 and N_2 is assumed to be zero ($\partial N_1/\partial t' = \partial N_2/\partial t' = 0$). With the abbreviations $N = N_1 + N_2$ (total concentration) and $n = N_1 - N_2$ (population difference) one obtains from Equations 51 and 52:

$$n = \frac{N}{1 + I_L/I_{S,2}} \tag{54}$$

with saturation intensity $I_{S,2}$ defined as

$$I_{S,2} = \frac{h\nu_L}{2\sigma_L \tau_F}. \tag{55}$$

Insertion of Equation 54 into Equation 51 gives the differential equation

$$\frac{\partial I_L}{\partial z'} = -I_L \sigma_L \frac{N}{1 + I_L/I_{S,2}} \tag{56}$$

The implicit solution of Equation 56 is

$$\ln\left(\frac{I_L(l)}{I_L(0)}\right) = \frac{I_L(0) - I_L(l)}{I_{S,2}} - \sigma_L N l. \tag{57}$$

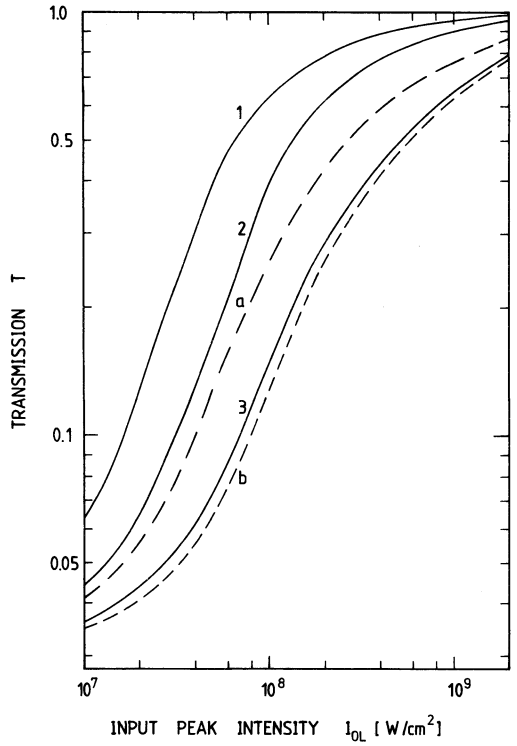

Figure 13 Comparison of two- and three-level steady state models with rigorous calculation. Parameters are listed in Table I. Curve 1: intensity transmission of steady state two-level model; curve a: corresponding energy transmission. Curve 2: intensity transmission of steady state three-level model with instantaneous decay from intermediate state; curve b: corresponding energy transmission. Curve 3: energy transmission corresponding to the level system of Fig. 3 and Equations 28–33.

Using the transmissions $T_0 = \exp(-\sigma_L N l)$ and $T = I_L(l)/I_L(0)$ an implicit transmission equation is obtained:

$$\ln\left(\frac{T}{T_0}\right) = \frac{I_L(0)}{I_{S,2}}(1-T). \tag{58}$$

The solution $T(I_{OL})$ is plotted in Fig. 13, curve 1. It deviates strongly from curve 3 which is calculated from the Equation system 28–33 (parameters of Table I). The S_1-state lifetime τ_F would be calculated to be a factor of four too short by fitting experimental points with Equation 58.

The two-level model is improved if the energy transmission T_E is calculated instead of T (Equation 37, in the experiments T_E is measured). The dashed curve (a) in Fig. 13 shows the result.

5.2. Steady state isotropic three-level system

The three-level system consists of states 1, 2 and 3 of Fig. 3. The isotropic differential equation system is

$$\frac{\partial I_L}{\partial z'} = -I_L \sigma_L (N_1 - N_2) \tag{59}$$

$$\frac{\partial}{\partial t'} N_1 = -\frac{I_L \sigma_L}{h\nu_L}(N_1 - N_2) + \frac{1}{\tau_F}(N_2 + N_3) \tag{60}$$

$$\frac{\partial}{\partial t'} N_2 = \frac{I_L \sigma_L}{h\nu_L}(N_1 - N_2) - \left(\frac{1}{\tau_F} + \frac{1}{\tau_{FC}}\right) N_2 \tag{61}$$

$$\frac{\partial}{\partial t'} N_3 = \frac{1}{\tau_{FC}} N_3 - \frac{1}{\tau_F} N_2. \tag{62}$$

The steady state condition requires that $\partial N_1/\partial t' = \partial N_2/\partial t' = \partial N_3/\partial t' = 0$. The total population is $N = N_1 + N_2 + N_3$ and the effective absorbing concentration is $n = N_1 - N_2$.

The steady state solution of n is [36]

$$n = \frac{N}{1 + I_L/I_{S,3}} \tag{63}$$

with the saturation intensity

$$I_{S,3} = \frac{h\nu_L}{\sigma_L \tau} \tag{64}$$

and the effective lifetime

$$\tau = \frac{2\tau_F \tau_{FC} + \tau_F^2}{\tau_F + \tau_{FC}}. \tag{65}$$

The solution of the intensity propagation Equation 59 is the same as in case of the two-level system (Equations 57 and 58) if $I_{S,2}$ is replaced by $I_{S,3}$.

The effective lifetime τ reduces to $\tau = 2\tau_F$ in the case of $\tau_{FC} \to \infty$ and the two-level case of Section 5.1 is obtained. For fast relaxation out of the excited Franck–Condon state $\tau_{FC} \to 0$, one obtains $\tau = \tau_F$.

Curve 2 in Fig. 13 depicts the intensity transmission $T(I_{OL})$ for the case of $\tau_{FC} = 0$. The curve is shifted to the right by a factor of two compared to the two-level system of Section 5.1 (curve 1). The corresponding energy transmission curve (b) represents a good approximation of the rigorously calculated curve 3 (Equations 28–33).

The energy transmission calculation T_E for the simple steady state three-level system with fast Franck–Condon state relaxation $\tau_{FC} = 0$ is applicable to the measurement of the S_1-state lifetime τ_F under the following conditions: (i) the pulse duration has to be more than a factor of three longer than the relaxation time τ_F; (ii) excited state absorption has to be negligible; (iii) intersystem crossing efficiency has to be small; (iv) the reorientation time τ_0 should be more than a factor of five shorter than τ_F.

In the example of Fig. 13 the three-level isotropic steady state energy transmission curve (b) and the generally calculated energy transmission curve 3 nearly coincide due to the fact that neglect of absorption anisotropy shifts curve (b) a factor of 1.5 to the right, while the assumption of steady state ($\Delta t_L \to \infty$) shifts the curve about the same factor to the left compared to $\Delta t_L = 25$ ps.

6. Conclusions

Various techniques for the determination of the S_1-state lifetime have been analysed. The complicated interaction of light with molecules in dye solutions is reduced to a system with a small number of levels. The advantages and disadvantages of fluorescence methods, stimulated gain measurements and absorption techniques have been discussed. The problem of single pulse bleaching is analysed by numerical methods and the influence of various pulse and dye parameters on the accuracy of the S_1-state lifetime measurement is estimated. Simple steady state isotropic two- and three-levels models are compared with rigorous numerical calculations. Each method has its limits and knowledge of the influence of various parameters on the measuring process for the lifetime detection is necessary to determine correct relaxation rates.

References

1. F. P. SCHÄFER (ed.), Vol. 1 'Topics of Applied Physics' (Springer, Berlin, 1977) pp. 1–83, 144–78.
2. S. L. SHAPIRO (ed.), 'Ultrashort Light Pulses' Vol. 18 of 'Topics in Applied Physics' (Springer, Berlin, 1977) pp. 18–81.
3. R. E. IMHOF and F. H. READ, *Rep. Prog. Phys.* **40** (1977) 1–104.
4. W. DEMTRÖDER, 'Laser Spectroscopy Basic Concepts and Instrumentation' Vol. 5 in Springer Series in 'Chemical Physics' (Springer, Berlin, 1981) pp. 546–584.
5. E. A. BAILEY and G. K. ROLLEFSON, *J. Chem. Phys.* **21** (1953) 1315–22.
6. R. D. SPENCER and G. WEBER, *ibid.* **52** (1970) 1654–63.
7. K. BERNDT, E. KLOSE and R. MÜLLER, in Proceedings of the Second International Symposium on Ultrafast Phenomena in Spectroscopy, October 30–November 5, 1980, Reinhardsbrunn, GDR, pp. 65–76.
8. D. SCHUBERT, H. WABNITZ and B. WILHELMI, *Exp. Tech. Phys.* **28** (1980) 435–42.
9. J. M. RAMSEY, G. M. HIEFTJE and G. R. HAUGEN, *Appl. Opt.* **18** (1979) 1913–20.
10. K. BERNDT, H. DÜRR and D. PALME, *Opt. Commun.* **42** (1982) 419–22.
11. R. R. ALFANO and N. OCKMAN, *J. Opt. Soc. Amer.* **58** (1968) 90–5.
12. G. R. HAUGEN, B. W. WALLIN and F. E. LYTLE, *Rev. Sci. Instrum.* **50** (1979) 64–72.
13. B. LESKOVAR, C. C. LO, P. R. HARTIG and K. SAUER, *ibid.* **47** (1976) 1113–21, 1122–9.
14. A. S. PINE, *J. Appl. Phys.* **39** (1968) 106–8.
15. M. E. MACK, *ibid.* **39** (1968) 2483–5.
16. R. I. SCARLET, J. F. FIGUEIRA and H. MAHR, *Appl. Phys. Lett* **13** (1968) 71–3.
17. R. CUBEDDU, S. DeSILVESTRI and O. SVELTO, *Opt. Commun.* **34** (1980) 460–2.
18. E. P. IPPEN, C. V. SHANK and A. BERGMAN, *Chem. Phys. Lett.* **38** (1976) 611–4.
19. E. G. ARTHURS, D. J. BRADLEY and A. G. RODDIE, *ibid.* **22** (1973) 230–4.
20. G. R. FLEMING, J. M. MORRIS and G. W. ROBINSON, *Australian J. Chem.* **30** (1977) 2337–52.
21. W. SIBBETT, J. R. TAYLOR and D. WELFORD, *IEEE J. Quant. Elect.* **QE-17** (1981) 500–9.
22. M. A. DUGUAY and J. W. HANSEN, *Appl. Phys. Lett.* **15** (1969) 192–4.
23. M. A. DUGUAY, in 'Progress in Optics' Vol. 14, edited by E. Wolf (North Holland, Amsterdam, 1976) pp. 161–93.
24. G. MOUROU, B. DROUIN, M. BERGERON and M. M. DENARIEZ-ROBERGE, *IEEE J. Quant. Elect.* **QE-9** (1973) 745–8.
25. H. MAHR and M. D. HIRSCH, *Opt. Commun.* **13** (1975) 96–9.
26. L. A. HALLIDY and M. R. TOPP, *Chem. Phys. Lett.* **46** (1977) 8–14.
27. B. KOPAINSKY and W. KAISER, *Opt. Commun.* **26** (1978) 219–24.
28. M. D. HIRSCH and H. MAHR, *Chem. Phys. Lett.* **60** (1979) 299–303.
29. G. S. BEDDARD, T. DOUST and G. PORTER, *Chem. Phys.* **61** (1981) 17–23.
30. S. J. STRICKLER and R. A. BERG, *J. Chem. Phys.* **37** (1962) 814–22.
31. G. W. SCOTT and L. D. TALLEY, in 'Advances in Laser Chemistry', edited by A. H. Zewail, Vol. 3 in Springer Series in 'Chemical Physics' (Springer, Berlin, 1978) pp. 187–94.
32. J. W. SHELTON and J. A. ARMSTRONG, *IEEE J. Quant. Elect.* **QE-3** (1967) 696–7.
33. M. M. MALLEY and P. M. RENTZEPIS, *Chem. Phys. Lett.* **3** (1969) 534–6.
34. M. R. TOPP, P. M. RENTZEPIS and R. P. JONES, *ibid.* **9** (1971) 1–5.
35. S. SCHNEIDER, E. LILL and F. DÖRR, in 'Picosecond Phenomena', edited by C. V. Shank, E. P. Ippen and

S. L. Shapiro, Vol. 4 Springer Series in 'Chemical Physics' (Springer, Berlin, 1978) pp. 23–6.
36. M. HERCHER, *Appl. Opt.* **6** (1967) 947–54.
37. C. R. GIULIANO and L. D. HESS, *IEEE J. Quant. Elect.* **QE-3** (1967) 358–67.
38. M. HERCHER, W. CHU and D. L. STOCKMAN, *ibid.* **QE-4** (1968) 954–68.
39. L. HUFF and L. G. DeSHAZER, *J. Opt. Soc. Amer.* **60** (1970) 157–65.
40. M. BERNSTEIN, L. J. ROTHBERG and K. S. PETERS, *Chem. Phys. Lett.* **91** (1982) 315–8.
41. V. A. BABENKO, V. I. MALYSHEV and A. A. SYCHEV, *Sov. J. Quant. Elect.* **6** (1976) 944–6.
42. V. A. BABENKO, G. G. DYADYUSHA, M. A. KUDINOVA, V. I. MALYSHEV, Yu. L. SLOMINSKII, A. A. SYCHEV and A. I. TOLMACHEV, *ibid.* **10** (1980) 1035–8.
43. Th. FÖRSTER, 'Fluoreszenz Organischer Verbindungen' (Vandenhoeck & Ruprecht, Göttingen, 1951) pp. 43–66.
44. J. LAVOREL, *J. Phys. Chem.* **61** (1957) 1600–5.
45. B. KOPAINSKY, J. K. HALLERMEIER and W. KAISER, *Chem. Phys. Lett.* **83** (1981) 498–502.
46. S. K. RENTSCH, D. FASSLER, P. HAMPE, R. DANIELIUS and R. GADONAS, *ibid.* **89** (1982) 249–53.
47. I. L. ARBELOA and P. R. OJEDA, *ibid.* **79** (1981) 347–50.
48. C. RULLIÈRE, *ibid.* **43** (1976) 303–8.
49. P. P. FEOFILOV, 'The Physical Basis of Polarized Emission' (Consultants Bureau, New York, 1961) pp. 108–71.
50. A. PENZKOFER and W. FALKENSTEIN, *Opt. Quant. Elect.* **10** (1978) 399–423.
51. J. WIEDMANN and A. PENZKOFER, *Il Nuovo Cimento* **63B** (1981) 459–69.
52. A. PENZKOFER and J. WIEDMANN, *Opt. Commun.* **35** (1980) 81–6.
53. B. P. BOCZAR and M. R. TOPP, in 'Picosecond Phenomena III', edited by K. B. Eisenthal, R. M. Hochstrasser, W. Kaiser and A. Laubereau, Vol. 23 in Springer Series in 'Chemical Physics' (Springer, Berlin, 1982) pp. 174–8.
54. W. BLAU, W. DANKESREITER and A. PENZKOFER, to be published.
55. M. E. MACK, *Appl. Phys. Lett.* **15** (1969) 166–8.
56. W. FALKENSTEIN, A. PENZKOFER and W. KAISER, *Opt. Commun.* **27** (1978) 151–6.
57. T. TAO, *Biopolymers* **8** (1969) 609–32.
58. H. E. LESSING and A. von JENA, in 'Laser Handbook' Vol. 3, edited by M. L. Stitch (North Holland, Amsterdam, 1979) Chap. B6, pp. 753–846.
59. J. M. DEMAS and G. A. CROSBY, *J. Phys. Chem.* **75** (1971) 991–1024.
60. D. von der LINDE and K. F. RODGERS, *IEEE J. Quant. Elect.* **QE-9** (1973) 960–1.
61. B. KOPAINSKY, W. KAISER and K. H. DREXHAGE, *Opt. Commun.* **32** (1980) 451–5.
62. R. W. EASON, R. C. GREENHOW and J. A. D. MATTHEW, *IEEE J. Quant. Elect.* **QE-17** (1981) 95–102.
63. W. BLAU, R. REBER and A. PENZKOFER, *Opt. Commun.* **43** (1982) 210–14.
64. D. FAUBERT and S. L. CHIN, *Can. J. Phys.* **57** (1979) 1359–61.
65. J. WIEDMANN and A. PENZKOFER, *Opt. Commun.* **30** (1979) 107–12.
66. W. LEUPACHER and A. PENZKOFER, *Appl. Phys.* **B29** (1982) 263–7.
67. K. B. EISENTHAL, *Ann. Rev. Phys. Chem.* **28** (1977) 207–32.
68. A. PENZKOFER, W. FALKENSTEIN and W. KAISER, *Chem. Phys. Lett.* **44** (1976) 82–7.
69. J. M. WIESENFELD and E. P. IPPEN, *Chem. Phys. Lett.* **67** (1979) 213–7.
70. C. V. SHANK, E. P. IPPEN and O. TESCHKE, *ibid.* **45** (1977) 291–4.
71. A. T. ESKE and K. RAZI NAQVI, *ibid.* **63** (1979) 128–32.
72. D. N. DEMPSTER, T. MORROW, R. RANKIN and G. F. THOMPSON, *ibid.* **18** (1973) 488–92.
73. W. RUDOLPH and H. WEBER, *Opt. Commun.* **34** (1980) 491–6.